

ADOPT: A tool for automatic detection of tectonic plates at the surface of convection models

C. Mallard, B. Jacquet, Nicolas Coltice

▶ **To cite this version:**

C. Mallard, B. Jacquet, Nicolas Coltice. ADOPT: A tool for automatic detection of tectonic plates at the surface of convection models. Geochemistry, Geophysics, Geosystems, 2017, 18 (8), pp.3197-3208. 10.1002/2017GC007030 . hal-02329271

HAL Id: hal-02329271

https://univ-lyon1.hal.science/hal-02329271

Submitted on 20 Dec 2021

HAL is a multi-disciplinary open access archive for the deposit and dissemination of scientific research documents, whether they are published or not. The documents may come from teaching and research institutions in France or abroad, or from public or private research centers.

L'archive ouverte pluridisciplinaire **HAL**, est destinée au dépôt et à la diffusion de documents scientifiques de niveau recherche, publiés ou non, émanant des établissements d'enseignement et de recherche français ou étrangers, des laboratoires publics ou privés.

Copyright

AGU PUBLICATIONS

Geochemistry, Geophysics, Geosystems

RESEARCH ARTICLE
10.1002/2017GC007030

ADOPT: A tool for automatic detection of tectonic plates at the surface of convection models

C. Mallard[1], B. Jacquet[2], and N. Coltice[1]

[1]Laboratoire de géologie de Lyon, École Normale Supérieure de Lyon, CNRS, Université de Lyon 1, Villeurbanne, France, [2]Kitware, Villeurbanne, France

Key Points:
- Detection of tectonic plates at the surface of convection models
- It is based on image segmentation techniques to detect objects
- The detection tool is effective to identify and close plate polygons even on diffuse plate zones

Correspondence to:
C. Mallard,
claire.mallard@univ-lyon1.fr

Citation:
Mallard, C., B. Jacquet, and N. Coltice (2017), ADOPT: A tool for automatic detection of tectonic plates at the surface of convection models, *Geochem. Geophys. Geosyst.*, *18*, 3197–3208, doi:10.1002/2017GC007030.

Received 22 MAY 2017
Accepted 26 JUL 2017
Accepted article online 11 AUG 2017
Published online 30 AUG 2017

Abstract Mantle convection models with plate-like behavior produce surface structures comparable to Earth's plate boundaries. However, analyzing those structures is a difficult task, since convection models produce, as on Earth, diffuse deformation and elusive plate boundaries. Therefore we present here and share a quantitative tool to identify plate boundaries and produce plate polygon layouts from results of numerical models of convection: Automatic Detection Of Plate Tectonics (ADOPT). This digital tool operates within the free open-source visualization software Paraview. It is based on image segmentation techniques to detect objects. The fundamental algorithm used in ADOPT is the watershed transform. We transform the output of convection models into a topographic map, the crest lines being the regions of deformation (plate boundaries) and the catchment basins being the plate interiors. We propose two generic protocols (the field and the distance methods) that we test against an independent visual detection of plate polygons. We show that ADOPT is effective to identify the smaller plates and to close plate polygons in areas where boundaries are diffuse or elusive. ADOPT allows the export of plate polygons in the standard OGR-GMT format for visualization, modification, and analysis under generic softwares like GMT or GPlates.

1. Introduction

Plate tectonic theory describes the plate tessellation at the Earth surface [*Morgan*, 1968]. The lithosphere is composed of about 50 rigid tectonic plates [*Bird*, 2003], which move over the surface. Since the 1990s, numerical convection models of mantle convection can generate self-consistent plate-like behavior [*Moresi and Solomatov*, 1998; *Trompert and Hansen*, 1998; *Tackley*, 2000, 2008]. These calculations have allowed to uncover that the plates layout depends on the models parameterizations [*Stein et al*., 2004; *Van Heck and Tackley*, 2008; *Foley and Becker*, 2009], and have helped to better understand dynamic feedbacks between mantle convection and the strength of the lithosphere [*Rolf et al*., 2012; *Mallard et al*., 2016].

It is now possible to compare the plate layout of convection models to that of Earth at present-day, or in plate tectonic reconstructions [*Morra et al*., 2013; *Mallard et al*., 2016]. However, building the plate layout of a convection model that produces continuous fields in essence, is a difficult and time-consuming task requiring careful analysis of various fields (velocity, seafloor age, viscosity, divergence, temperature), and picking plate boundaries by hand using for instance the GPlates software [*Williams et al*., 2012]. Difficulties arise for regions where deformation is diffuse and where it is necessary to close a plate polygon. Such problems exist also on Earth since a fraction of the surface involves diffuse or elusive deformation [*Gordon*, 1998]. *Bird* [2003] shows how plate boundaries are more complex than the classical trio ridge-trench-transform, and that some arbitrary choices have to be made in some places because plate tectonics theory applies for perfectly rigid plates only.

In this study, we propose and share a digital tool, ADOPT, to automatically detect plate boundaries and generate the plate polygons within the free open-source Paraview software [http://www.paraview.org]. This tool is based on an image segmentation processing algorithm: the watershed detection developed by [*Beucher and Lantuéjoul*, 1979]. It offers the possibility to preprocess the data with a nonmaximum suppression algorithm [*Canny*, 1986] to detect nondiffuse plate boundaries. ADOPT produces plate layouts with closed polygons ready to be exported into a OGR-GMT format, operated by common softwares like GMT [*Wessel et al*., 2013] or GPlates. The first step of ADOPT is to transform the information from a convection model into an elevation map, and we propose two different methods to do so. The second step is to determine the catchment basins of this elevation map, corresponding ultimately to tectonic plates through the

© 2017. American Geophysical Union. All Rights Reserved.

watershed algorithm. To evaluate the consistency of the methods, we compare the automatic extraction of plate layout with the detection based on visual inspection published in *Mallard et al*. [2016], for which diffuse deformation and elusive plate boundaries exist.

2. Materials and Methods

The automatic tool for tectonic plates detection on the surface of convection models called ADOPT runs through the visualization software Paraview. It is based on the watershed transform, which detects catchment basins from an elevation map. To apply this transformation, we have to convert the surface of a convection model into an artificial elevation map (not the true topography produced by density differences and convective flow). The higher elevations values (i.e., crests) have to correspond to the locations of plate boundaries. The users need to combine visual inspection with ADOPT to check the quality of the results.

2.1. Input: Fields Produced by 3-D Convection Models

The substrate of ADOPT is any surface (Cartesian, spherical, bumpy. . .) selected with the Paraview tools (slice, extract surface, contour) from a numerical convection model output. ADOPT is not code-specific, and can be used with results produced by any numerical code (see examples in Discussion), and only requires production of files readable by Paraview (.vts, .vtu, .vtk for instance). The resolution needs to be relatively homogeneous over the surface. ADOPT works on any discrete field as long as lateral gradients of the field are strong across what corresponds to a plate boundary. Therefore the field can be continouous or not.

2.2. Segmentation Algorithm: The Watershed Transform

The determination of the plate boundaries at the surface of numerical convection models is a problem of morphological segmentation. These problems are extensively treated in image processing, using topographic distance (distance along the relief) to detect objects. The watershed transform method is the principal tool of morphological segmentation. Therefore we choose this efficient method [*Meyer*, 1994; *Najman and Schmitt*, 1994; *Meyer*, 2012] to obtain consistent automatic closed contouring of plates. The key to apply the watershed transform is to transpose field values into an elevation field of which its crests and catchment basins are the objects to detect. Here, crests are potential plate boundaries, and catchment basins are plate interiors.

Once we have a potential topographic surface, the principle is to determine the minima, which are each associated with catchment basins. Indeed, each catchment basin contains one and only one connex region of minimum elevation. One minimum is labelled the deepest neighbor. The watershed lines (here plate boundaries) are like dams between catchment basins (here tectonic plates). The watershed lines are obtained by gradually flooding the surface, starting from the local minima. During the progressive flooding, a piece of dam is built on points where two or several floods would merge. When flooding is complete, only the dams emerge [*Meyer and Beucher*, 1992; *Dougherty*, 1994]. Nevertheless, we might want to ignore small basin or puddle, if they are not deep enough, depending on a "flooding threshold," which determines the sensitivity of the detection. A basin with a local water depth below that threshold is merged with its neighbor, avoiding excessive detection of watershed lines. Therefore, the number of plates decrease with increasing flooding threshold. One obstacle to a successful segmentation is the roughness at low elevation due to intraplate deformation, which can lead to oversegmentation.

2.3. Paraview Plugins

ParaView is a free open-source software for visualization and analysis of complex 2-D/3-D data such as 2-D or 3-D images, and structured/unstructured meshes. It is a classical high-performance software for mantle convection modelers. Paraview is a desktop and server application that can be used with large data sets on a laptop or a supercomputer using distributed processors and memory. Paraview is a Graphical User Interface (GUI) around the open-source framework VTK (Visualization toolkit). We developed plugins containing filters for our workflow, which we describe in the following section.

These plugins include the following Paraview filters:

1. "NonMaximumSuppression For Unstructured Data Set" which is the nonmaximum suppression operation working on a data set. It sets to 0 the values of nodes which are not maximum according to the direction of a vector field.

2. "HysteresisThreshold for Unstructured Data Set," working on a data set, which sets all values above a first threshold to the value of this threshold. It also sets to 0 the values that are above a second threshold (lower than the first one) if the corresponding node is connected to a node having a value over or equal to the first threshold.
3. "Watershed For Unstructured Data Set" which is the watershed segmentation with merging threshold, working on a data set. The merging threshold corresponds to the minimum depth required for a basin to be considered as a catchment basin. The value of the threshold is the percentage of the maximum depth of a basin in the data set, being the difference between the maximum and minimum elevation in the data set. It outputs a new field providing each cell an ID corresponding to the catchment basin it belongs to. When changing the merging threshold, the filter keeps in memory the IDs of basins that are merged.
4. "PolyDataExplodeToMultiblock" which splits a mesh with multiple fields (called polydata) to separate meshes i.e., a multiblock, based on the values of a field the user specifies.
5. A plugin to export plate boundaries into OGR-GMT shapefile (GMT ASCII Vectors). The OGR-GMT is a classical standard for digital plate boundary models. This is included as a possible format within the Save Data operation.

Until the plugins are integrated in the regular version of Paraview, we have deployed a virtual machine and a software container, both with the plugins installed and a version of Paraview on which they are effective. Therefore, Paraview and the ADOPT plugins are implemented as self-contained systems that guarantees they will always run the same, regardless of where it is deployed. The virtual machine runs with VirtualBox (http://www.virtualbox.org/), and Docker (http://www.docker.com), the software container platform, can be found along with the files used here on the open data repository https://osf.io/dfzwn. When running VirtualBox, the user launches Paraview and loads the following plugins to operate: GeodesicMeasurement, which is already in the plugin list, and libEarthPolylineWriter.so, libHystresisThresholdAndNonMaximumSuppressionUnstructuredDataset.so, and libWatershedUnstructuredDataset.so which are in the directory/home/ucbl/UCBL-PV-Build/. Unfortunately, the virtual machine uses the processor of the local computer to render the images, not the graphics card. So we suggest to prepare the data so the file represents only the surface to work on, and not the full 3-D volume of the model. Working on a surface, even dense in nodes, is efficient on a present-day laptop. With Docker, ADOPT runs on the graphics card.

2.4. The Segmentation Workflows

We define below workflows to automatically detect plates under Paraview. We detail both the field and distance methods using the logarithm of the viscosity at the surface of convection model (Figures 1 and 2). This example is relevant for pseudo-plastic models. In the snapshot of the models we present, low viscosity correspond to nodes where yielding occurs, and they are expected to be plate boundaries. High viscosities are supposed to be in the interior of plates. These workflows can be applied to any type of scalar fields or transformation of them, as long as they are relevant to detect plate boundaries. The strain rate and velocity magnitude, as we see in the next section, are some good examples in practice.

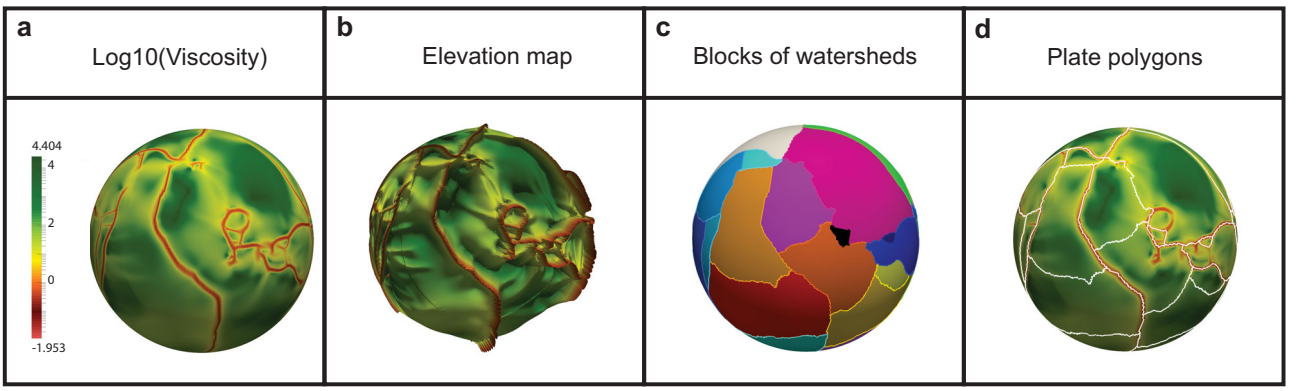


Figure 1. Sequential steps to perform the field method, using a snapshot of the surface viscosity field of a numerical convection model from *Mallard et al.* [2016], the yield stress being here 150 MPa. (a) Logarithm of the nondimensional viscosity field; (b) Elevation map corresponding to Figure 1a; (c) Result of the watershed transform with a threshold of 4%: the different colors show the blocks representing the detected plates. (d) Plates polygons geometries ready to be exported into the OGR-GMT format.

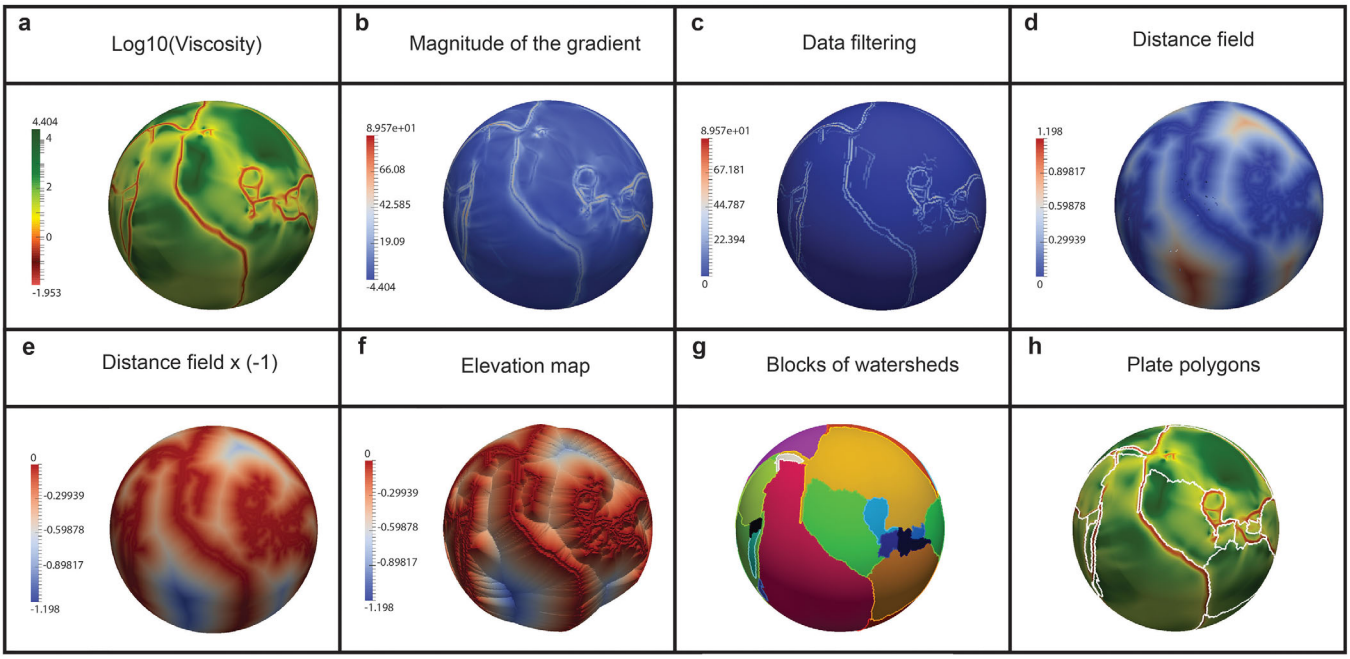


Figure 2. Sequential steps to perform the distance method, using the same snapshot as in Figure 1. (a) Logarithm of the nondimensional viscosity field; (b) Magnitude of the gradient of the field (a); (c) Results of the hysteresis threshold filter (thresholds are 80 and 8) and result of the non maximum suppression. (d) Conversion of Figure 2c into the distance field; (e) Change the sign of the field (d) to obtain the high values as crest; (f) Elevation map; (g) Result of watershed transform with a threshold of 4%: the differents colors show the blocks representing the different mesh per plates. (h) Plates polygons geometries ready to be exported into the OGR-GMT format.

2.4.1. The "Field" Method

This method does not involve preprocessing the data (Figure 1). The elevation map on which we apply the watershed filter is the selected field (the logarithm of the viscosity in Figure 1) produced by the convection model. The workflow is as follow:

1. Extract the surface of the 3-D spherical convection model using the filter "extract surface."
2. Apply the filter "Watershed For Unstructured Data Set" on the extracted surface to identify the catchments basins i.e., tectonic plates (Figure 1c).
3. Apply the filter "PolyDataExplodeToMultiblock," which takes all the cells that have the same ID and store them in a separate mesh (Figure 1c).
4. Apply the filter "Feature edges" on the meshes to group the boundaries edges. Apply the filter "triangle trips" to reconnect two edges that share a node. Therefore, every catchment basin defines a plate polygon (Figure 1d). Export the polygons to the OGR-GMT format, ready to be visualized and analyzed with GMT or GPlates.

2.4.2. The "Distance" Method

In this method (Figure 2), we produce the elevation map which corresponds to the distance from each point to the closest point with nonzero value of a given field. In the example, this given field being the gradient-magnitude of the logarithm of the viscosity. We assume that the strong gradients of the chosen field correspond to potential location of plate boundaries because the viscosity drops where deformation localizes. Hence, we first compute the gradient of the field. We then apply the nonmaximum suppression filter. It is an edge detection technique to select lines of maximum values. On the latter field, we apply a hysteresis threshold filter. Hence we select nodes with values above the maximum threshold. We also select those above the minimum threshold only if they are connected to maxima. That eliminates the data that cannot be consider as plate boundaries a priori. Then we convert the result field into a new field in which all the nonmaximum data (interior of plates) are equal to 0. At this stage, the identified boundaries may not be sufficient to define closed plate polygons, because diffuse or very small deformation may exist. Therefore, we produce a new field, which is the geodesic distance from the position of cells to their closest maximum. Then, this distance field is used as the topographic map to apply the watershed segmentation.

The workflow under Paraview is:

1. Extract the surface of the 3-D spherical convection model using the filter "Extract surface."
2. Compute the gradient of the field with the filter "Gradient of unstructured data" (Figure 2b).
3. Isolate the crest lines applying the filter "NonMaximumSuppression For Unstructured Data Set" to the gradient field, which sets nonmaximum nodes, according to the direction of the gradient, to 0 (Figure 2c) and apply the filter "HysteresisThreshold for Unstructured Data Set," and fix the two threshold values. The first threshold corresponds to a value over which it is certain that a node belongs to a definite plate boundary. The second threshold corresponds to the value of data to keep for which node is connected to a definite plate boundary. Hence, data having values below the second low threshold are defined as nonplate boundaries. A node having a value between these two thresholds can belong to a plate boundaries if it is connected to a node which value is above the first threshold. Adjust carefully the threshold values with a criterion of choice depending on the model.
4. Apply the filter "Fast-Marching Geodesic Distance-Field From Binary Field" to generate the distance field on the sphere (Figure 2d). From the binary field, we find the distance to the nearest crest using the fast marching method [*Sethian*, 1999].
5. Multiply by (–1) using the calculator to generate the corresponding the elevation map (Figure 2e) because we want the highest elevation to correspond to the distance 0.
6. Apply the filter "Watershed For Unstructured Data Set" on the extracted surface to identify the catchments basins (Figure 2f).
7. Apply the filter "PolyDataExplodeToMultiblock." It takes all the cells that have the same ID and store them in a separate mesh, which is cut into several meshes corresponding to the catchment basins i.e., tectonic plates (Figure 2g).
8. Apply the filter "Feature edges" on each meshes to group the boundaries edges. Apply the filter "Triangle trips" to reconnect two edges that share a node. Therefore, every catchment basin define a plate polygon (Figure 2h). Export the polygons to the OGR-GMT format, ready to be visualized and analyzed with GMT or GPlates.

2.4.3. Differences Between the Two Methods

The major difference comes from the roughness of the elevation maps. In the field method, the variations of the elevation depend on the maximum and minimum values of the data. Since the relevant fields involve strong gradients, the field method generates rugged relief (Figure 1b). Therefore, some crests may not be high enough to end up being detected as plate boundaries. Additionally, plates with strong internal deformation may correspond to deep catchment basins using the viscosity or strain rate fields for instance. Therefore, although the boundaries are easily detected visually, the watershed transform may not detect them for high values of the threshold.

In contrast, the distance field method produces a smooth elevation map because the distance from the location to the nearest local maximum evolves more or less linearly (Figure 2f). Because of the method to compute the distance, a small local maximum in terms of the field produced by the convection model, has the same importance as a large one. In contrast, the minima and maxima of the elevation map for the field method represent physical values that vary laterally. Therefore the two methods give different elevation maps, and hence potentially two different watershed segmentations where deformation is small or diffuse.

In the following section, we compare the plate polygons obtained with these two methods and by visual inspection. Thanks to this evaluation, we will determine the appopriate conditions to use each of these methods.

3. Testing ADOPT Against Detection by Visual Inspection

3.1. The Data

The plate detection software perfectly detects plates for a field describing polygons with sharp discontinuous boundaries. Hence, the real and informative test is to detect plate polygons from a continuous field with diffuse and elusive boundaries. Therefore, we test now the tectonic plate detection method on two 3-D spherical models of mantle convection displaying a plate-like behavior. We use here the 3-D spherical models of *Mallard et al*. [2016], because we can compare the plate polygon configurations presented in that article to those produced with ADOPT. These 3-D spherical convection models are produced with the code

StagYY, solving for the nondimensional equations of mass, momentum, and heat conservation on an Yin-Yang grid [*Tackley*, 2008]. The pseudo-plastic rheology is an empirical approximation of the mechanical behavior of the mantle-lithosphere system [see *Coltice et al*., 2017 for a review]. It is designed to generate plates self-consistently. We select two snapshots (called YS150 and YS250) corresponding to models with a yield stress of 150 and 250 MPa, respectively (Figures 3 and 4). The plateness as defined by *Zhong et al*. [1998] is 0.75 and 0.81, respectively. A 90% of the surface deformation lies within $<$15% of the surface area. We choose those two models because (a) they both have plate layouts with Earth-like properties (one distribution of the area of large plates and a fragmentation distribution of small plates), and (b) they correspond to two extreme cases of plate geometries: in YS150 plate boundaries are numerous and well defined, but plate interiors display some degree of deformation; in YS250 deformation within plates is very limited, but some plate boundaries are wide and diffuse. The details of the models are presented elsewhere [see *Mallard et al*., 2016].

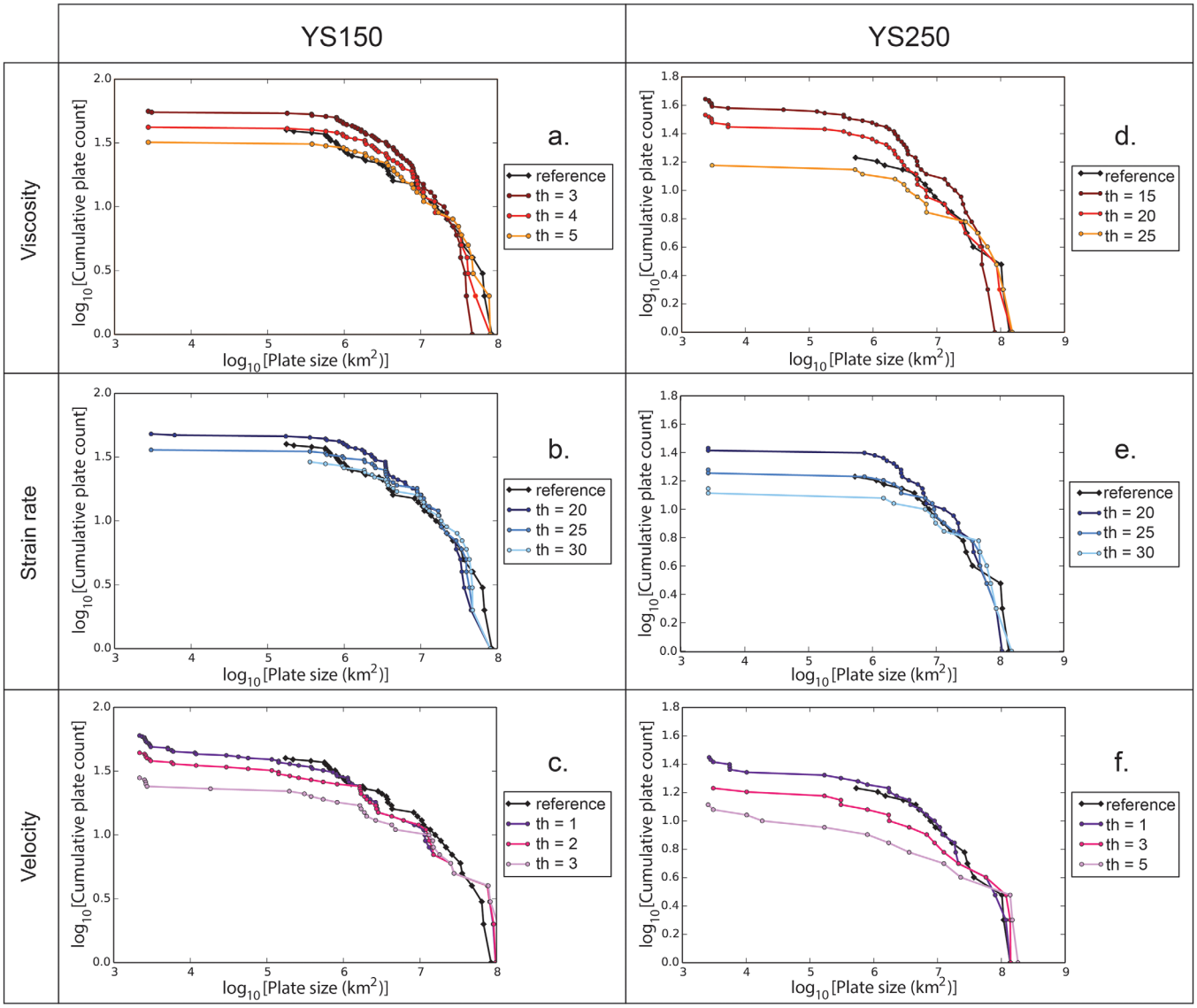


Figure 3. Plots of the logarithm of cumulative plate count versus the logarithm of plate size for YS150, YS250 with the field method and the references. The cumulative plate count represents the number of plates that exceed a given area. The graphs show the automatic layout extraction from the viscosity, strain rate, and velocity fields for the convection models. Each graph represents the results obtained with three different watershed thresholds (th). The colors represent the different fields used: red for the viscosity, blue for the strain rate, and pink for the velocity. The black curve represent the data obtained by visual inspection.

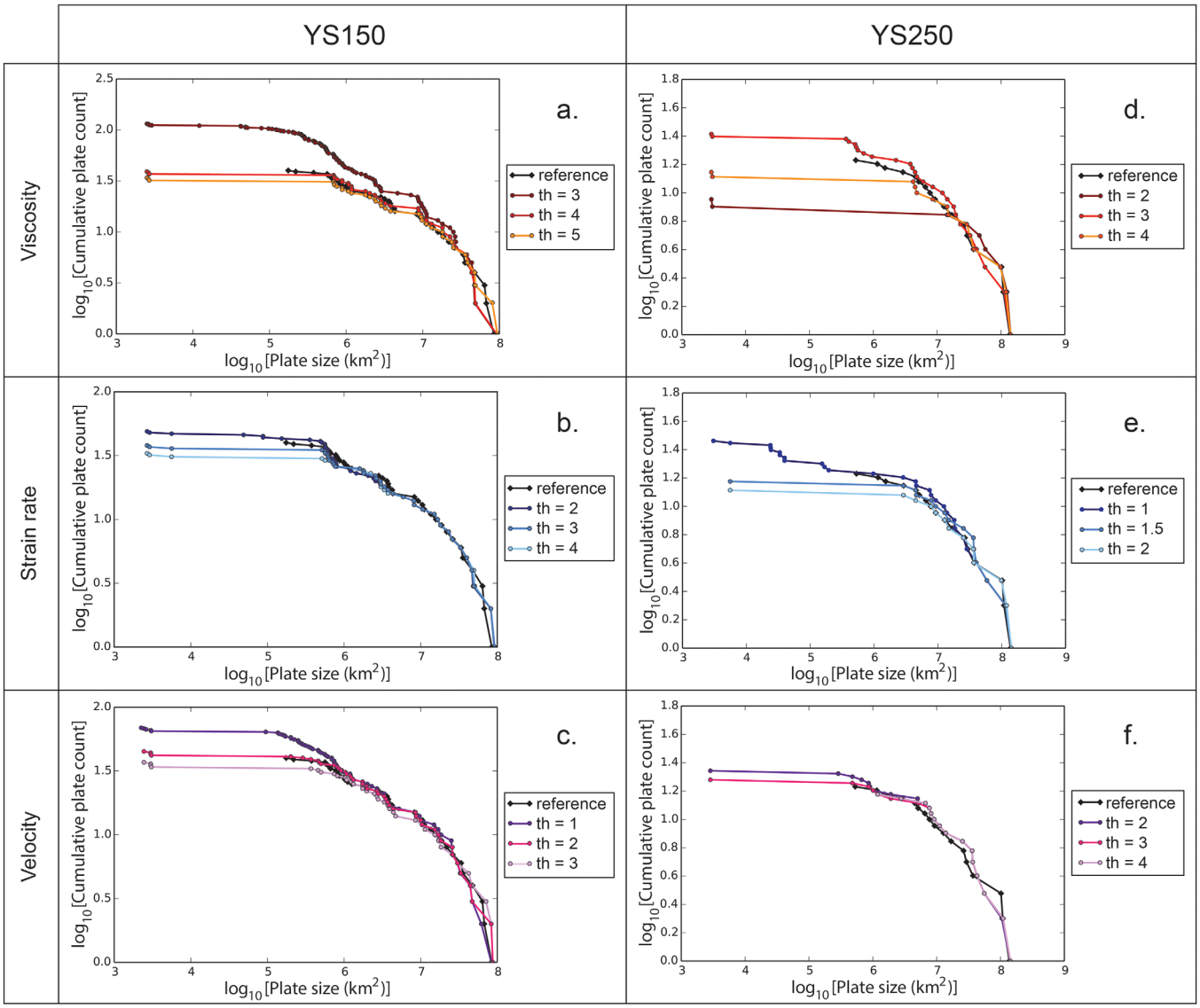


Figure 4. Plots of the logarithm of cumulative plate count versus the logarithm of plate size for YS150, YS250 with the distance method and the references. The cumulative plate count represents the number of plates that exceed a given area. The graphs show the automatic layout extraction from the viscosity, strain rate, and velocity fields for the convection models. Each graph represent the results obtained with three different watershed thresholds (th). The colors represent the different fields used: red for the viscosity, blue for the strain rate, and pink for the velocity. The black curve represent the data obtained by visual inspection.

We consider the corresponding plate layouts, realized from visual inspection and independently to the present study, as the references. In this previous work, they used plate tectonics rules to determine the plate boundaries using GPlates. *Mallard et al.* [2016] digitized the plate boundaries polygons through a careful analysis of several fields from our model outputs: surface velocity, horizontal divergence, viscosity, synthetic seafloor age, and temperature.

We compare the results of the automatic detection to the reference layouts produced manually. Although called the reference, the layout produced from visual inspection suffer some limitations too in regions of diffuse deformation, or where elusive plate boundaries are necessary to close a polygon. We therefore compare the abilities of ADOPT to solve quantitatively problems to close polygons in regions where it is a difficult task. We extract the plate tessellation processing separately three different fields of the convection models: the viscosity, the strain rate, and the magnitude of the velocity, with three different values of threshold for the watershed transform. We worked on the logarithm of the viscosity and strain rate instead of the fields themselves because the methods needs strong gradients, but weak roughness to avoid oversegmentation. Because lateral variations of viscosity in these models are up to 6 orders of magnitude, the

logarithm of the viscosity already displays strong gradients, and it smoothes the roughness that is large for the field itself. This choice was made on try and error tests, and may not be relevant to other models.

3.2. Cumulative Number Versus Area Distribution of Plates

3.2.1. The Field Method

Figure 3 displays the plate-size distributions obtained using the field method, and the reference distribution. The reference does not propose plates of area lower than 10^5 km^2, because of the difficulty to identify small plates by visual inspection. Microplates of area $<$0.0006% of the total surface can be detected with the automatic detection depending on the threshold of plate area for the watershed transform (Figures 3 and 4). The lower the threshold, the smaller the plates can be. With this method, the value of the threshold, corresponding to the percentage of the maximum depth of a basin in the data set, can reach 30% (see Figure 3). Such high values express the fact that the direct conversion of the field to elevation can produce very sharp cliffs (Figure 1c). Therefore, very small catchment basins with large depths can exist. Merging them to the appropriate catchment basin automatically can require to increase the threshold to a large percentage of the elevation gap in the data set. For some fields such as the magnitude of the velocity, thresholds lower than 10% are effective to produce a plate area distribution consistent with the manual detection of plates (Figure 3 bottom).

As expected, increasing the threshold of the watershed decreases the number of plates for all setups. However, we observe different sensitivities to the threshold of the watershed depending on the nature of the field used. Indeed, the plate-size distributions obtained from the velocity and the viscosity fields are more sensitive to a change of threshold than the distribution obtained from the strain rate.

When the threshold decreases, splitting of catchment basins is favored, decreasing the number of large plates ($>$12 10^6 km^2) and increasing the number of average and small plates. The data obtained from the viscosity field of YS150 (Figure 1a) illustrate this property. For YS250 (Figure 3d), there is just a sole microplate when the threshold is increased to 25%.

Small and average plates are easily detected for YS150 because it presents less broad zones of diffuse deformation than YS250 (Figure 3a). The best result for large plates and small plates distributions are obtained using the magnitude of the velocity, with additional detection of microplates.

The fits are better for YS250 than for YS150, because intraplate deformation in the former model is lower than in the latter (Figures 3d–3f). For large and intermediate plates, the distributions obtained from the velocity are quasi identical to the reference for both YS150 and YS250 (Figure 3f). However, the distributions of micro and small plates obtained from the strain rate field show a slightly better fit than for other fields (Figure 3e). Using the magnitude of the velocity is more effective to detect plate boundaries where deformation. The viscosity and strain rate fields do not produce strong enough contrast in regions where velocity variations are small (diffuse deformation).

3.2.2. The Distance Method

Figure 4 depicts the distribution of plate area obtained with the distance method. The effect of the threshold of the watershed is similar: increasing it leads to less micro and small plates. The fit is similarly good for all fields of YS150 (Figures 4a–4c). The large plates do not have identical sizes to those of the reference, but overall the fits are better than with the field method. The distribution of plates obtained from the strain rate (Figure 4b) is slightly more accurate than for other fields for YS150.

The distance method applied to YS250 generates too many small and microplates when using the viscosity field (Figure 4d) and the strain rate field (Figure 4e). For the later, numerous microplates disappear when the threshold is increased to 1.5%. The plate distribution obtained from the velocity field (Figure 4f) gives the best fit for YS250.

3.3. Plate Topology

Depending on the method used, the plate topology can slightly vary, as seen in Figure 6. Here, the best solution corresponds to the plate layout obtained with the distance method using the magnitude of the velocity. The differences between the layouts obtained with that field and the others are small: with the field method, some small plates are neglected, and some very large plates are split into two large plates. In the cases we tested, the threshold of the watershed filter has the bigger impact for plate oversight or splitting.

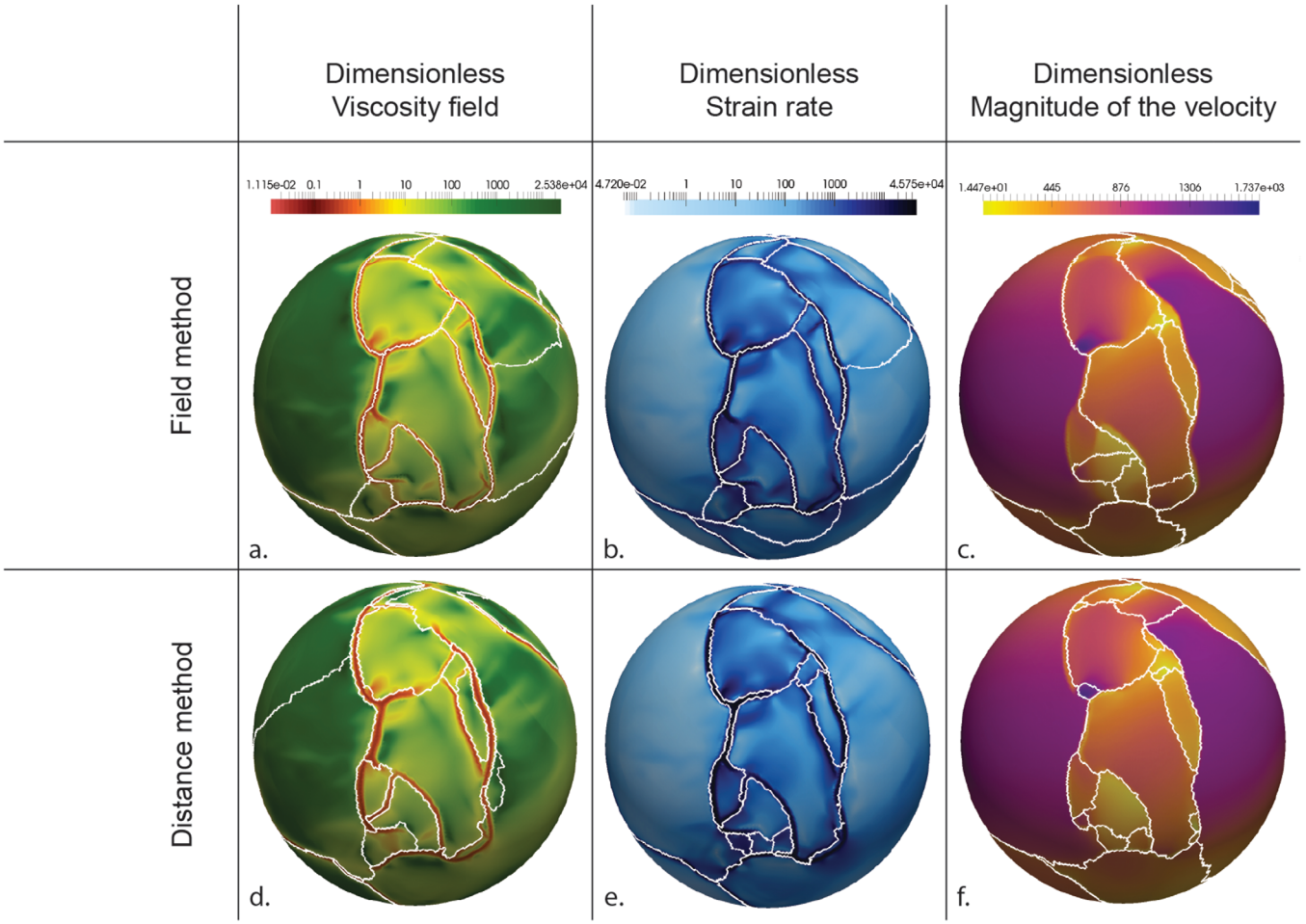


Figure 5. Snapshots of the nondimensional viscosity, strain rate, and velocity fields of the surface of the numerical convection model YS150. The plate boundaries in white are automatically detected with the field method (a, b, c) and the distance method (e, f, g).

For the distance method, the plate boundaries are not well defined for the viscosity and strain rate fields (Figure 5). This is because our convection models produce plate boundaries that are wider than expected on Earth.

The comparison between the reference layout and that produced with the distance method using the magnitude of the velocity shows ADOPT detects accurately the plate boundaries of large plates detected by visual inspection, but also for smaller ones (Figure 6). The tendency is to detect plate boundaries of small plates at different locations than the reference, but only for regions of diffuse plate boundaries and restricted back-arc opening. ADOPT also helps detect plate boundaries for which visual detection becomes subjective. It expresses the difficulties to visually position a plate boundary in regions of diffuse deformation, or where it is required to close a polygon although there is no unequivocal localization of deformation.

4. Discussion

We proposed a methodology, based on the watershed segmentation method, to detect automatically closed polygons corresponding to tectonic plates at the surface of convection models with plate-like behavior. The watershed transform produces a perfect layout if plates are perfectly rigid, but its strength is to produce closed polygons even if diffuse deformation or some elusive plate boundaries exist in the problem. To evaluate the method, we compared the statistics of the plate distribution and the layout produced for two models for which plate layouts build visually are published [*Mallard et al.*, 2016]. These reference models display diffuse deformation and wide regions of localized deformation, therefore they constitute a strong

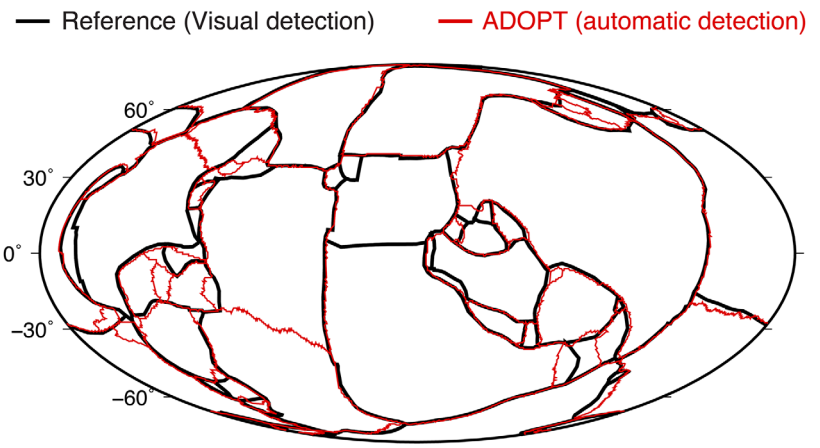


Figure 6. Automatic detection of plate polygons (distance method using the magnitude of the velocity) at the surface of the numerical convection model YS150, versus the visual detection of *Mallard et al*. [2016].

test. We propose two methods to apply on fields produced by the convection models. Both methods identify the pattern of plate tessellation, producing a distribution of plate area similar to the Earth, and to what was found from visual inspection. However differences exist between the field method and the distance method, and differences also exist with the reference plate layouts.

After selecting the best fits to the manual detection, for each automatic detection, both the field and distance methods provide accurate detections when the surface has a lot of plate boundaries (YS150) and with large zones of diffuse deformation (YS250). Preprocessing the data with the nonmaximum suppression and the hysteresis threshold filters, before applying the watershed transform, produces less detection of microplates in the distance method (Figures 7c and 7d) than in the field method. The distance method fits better the reference distribution than the field method.

In Figure 5, we observe that some obvious plate boundaries are neglected using the field method (Figures 5a–5c), but in majority, plate boundaries are defined accurately where deformation is localized. An issue with the field method is that if detected crests circumscribe a region of deformation, the catchment basin is

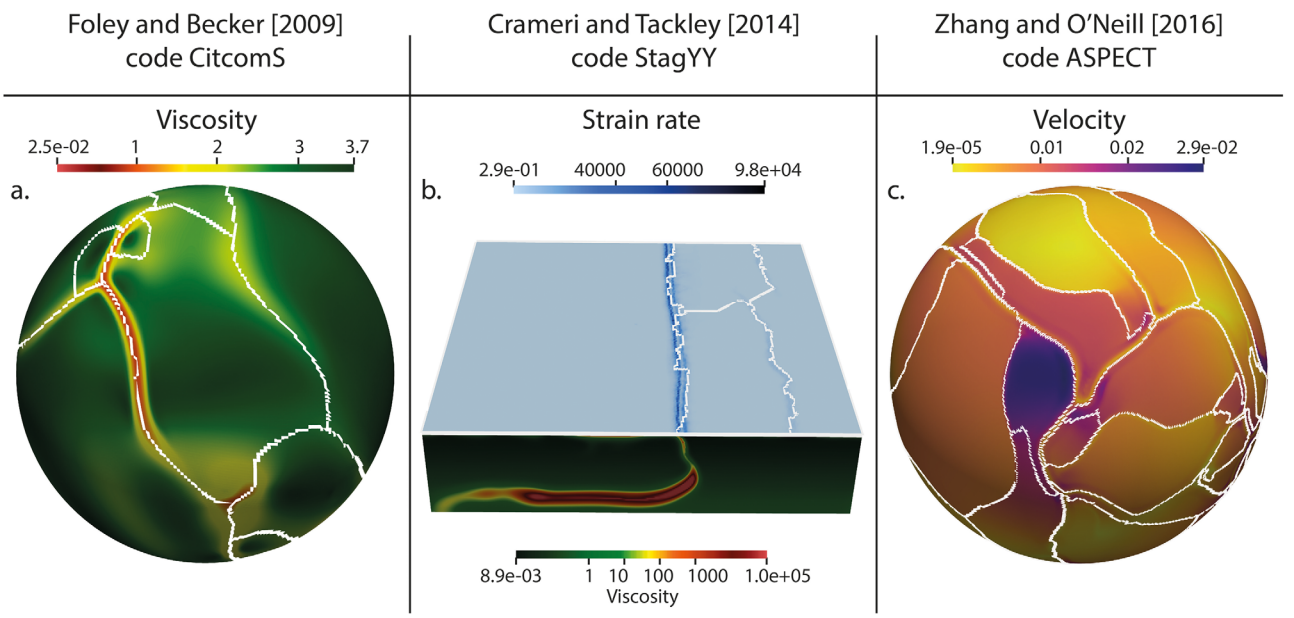


Figure 7. Snapshots of the viscosity, strain rate, and velocity fields of the surface of three different numerical convection models obtained with three different codes. The plate boundaries in white are automatically detected with the distance method. (a) Output from *Foley and Becker* [2009] computed with the code CitcomS. (b) Output from *Crameri and Tackley* [2014] computed with the code StagYY. (c) Output from *Zhang and O'Neill* [2016] computed with the code ASPECT.

omitted because its depth is below that of the threshold of the watershed transform. The distance methods avoids this issue, but if the numerical model of convection produces wide plate boundaries, then the automatic detection potentially places the contours of plates at their edges where gradients are the strongest (Figures 6d and 6e). Using the magnitude of the velocity field for the detection seems to avoid this problem (Figure 6f). We suggest that users of ADOPT try both methods and use the visual inspection to determine the more appropriate one.

There are differences between the layouts produced with ADOPT and those produced by visual inspection of a diversity of fields. Some of them come from the limitations of ADOPT we discussed previously, some come from the characteristics of the convection models. Indeed, the models presented here do not produce plate boundaries as sharp as on Earth. With a better description of the rheology [see *Crameri and Tackley*, 2015; *Coltice et al*., 2017], the improved sharpness of plate boundaries allows more accurate detections. Although taken as a reference, the detection from visual inspection are not necessarily an ideal solution, because *Mallard et al*. [2016] acknowledge the existence of diffuse plate boundaries and difficulties to close some polygons. The detection by visual inspection was realized with more information than what we use here. Combining several fields in appropriate manner could lead to an abstract field that provides a better expression of the plate boundaries.

ADOPT works on outputs of any convection codes and on any geometries, as long as they are readable by Paraview (Figure 7). The sole limitation of its use, regardless of the quality of the results, is the heterogeneity of the mesh resolution. For example, we could not produce plate layouts with ADOPT on the model of *Stadler et al*. [2010] produced with the code Rhea. Adaptative mesh refinement generates a factor of 5 of variations of the resolution at the surface, from 1 to 5 km. However, we successfully tested the automatic detection on three different results with homogeneous meshes of 3-D convection models. Figure 7a shows the results of *Foley and Becker* [2009] computed using the spherical shell convection code CitcomS [*Moresi and Solomatov*, 1998]. Figure 7b shows a calculation in Cartesian geometry with sticky air with the code StagYY from *Crameri and Tackley* [2014]. The zigzag observed on the high strain rate values are due to the width of the deformation area close to the trench. Figure 7c shows an output from *Zhang and O'Neill* [2016], which simulate the mantle flow of Mars-like planete built upon the open source finite element code ASPECT [Bangert et al., 2017]. The precision of the produced layouts and the detections of plates depend on the platness of the models.

The automatic plate detection tool we propose generates plate polygons although the fields over which it operates can be continuous. Therefore, there is no perfect solution to obtain. The tool allows to save a substantial amount of time, but it is necessary to examine the results and potentially operate corrections by hand, using additional knowledge or taking into account the limitations of the numerical models of convection used. The export tool we implemented is essential in that manner, since the produced files in the OGR-GMT standard can be imported in GPlates for modifications. Our algorithm does not forbid the detection of plates within plates. If one encounters such configuration, for instance, correcting the layout with GPlates may be required.

5. Conclusions

We have developed ADOPT, a digital tool to identify tectonic plates at the surface of the convection models from continuous fields produced. The automatic detection of the plate boundaries, hence the plate polygons, relies on a watershed transform algorithm, classically used for image segmentation. We implemented plugins and filters to realize the automatic plate detection in the free open-source software Paraview, and we share the source codes, and the reference plate polygons detected by visual inspection for testing. We have deployed both a VirtualBox and a Docker container as a tools to ensure sustainability of the tools, and efficient usage regardless of the operating system one uses. The data files, the virtual machine file, and the Docker files can be found here: https://osf.io/dfzwn.

We developed two different protocols to use ADOPT efficiently: the first one is based on the detection directly on the surface values of fields produced by the convection models. The second one is based on the conversion of the surface data into a distance field. Automatic detection of plates relies on one parameter: the watershed threshold which corresponds to the percentage of the maximum depth over which a catchment basin, i.e., a plate, is considered. We compared the results with plates geometries obtained from automatic detection and visual inspection.

Both protocols give plate layouts fitting well the cumulative plates versus plate-size distributions obtained by visual inspection. However, the distance method gives a better fit than the field method. Using the distance method on the magnitude of the velocity field gives the more consistent plate geometry for the considered models. Although, combining different fields and operations on them could lead to more appropriate solutions. For both methods and the various fields we used, a subsequent visual check is necessary because some limitations persist depending on the sharpness of deformation regions in the model produced, and intrinsic capabilities of the watershed algorithm. Thanks to the export tool into the OGR-GMT standard, it is possible to correct the plate layouts with the GPlates software in an optimal way.

Despite limitations, ADOPT is an effective tool that saves a substantial amount of time to study the evolution of plate layouts of convection models with plate-like behavior, allowing comparison with the data for plate tectonic reconstructions [*Bird*, 2003; *Morra et al*., 2013]. It provides means to quantitatively evaluate the similarity between the surface dynamics of the Earth and convection models.

Acknowledgments
We thank Thorsten Becker, Fabio Crameri, Giampiero Iaffaldano, and an anonymous reviewer for constructive comments that helped improve the manuscript. We could not test ADOPT on other codes without the help of Georg Stadler, Siqi Zhang, and Craig O'Neill, Fabio Crameri, Brad Foley, and Thorsten Becker. They kindly shared their data in the needed format. Finding some from almost 10 years ago is a challenge. We appreciate a lot and thank them very much. The research leading to these results was funded by the European Research Council within the framework of the SP2-Ideas Programme ERC-2013-CoG under ERC grant agreement 617588. The Virtual Box file and the Docker files can be found along with the data used here on the open data repository https://osf.io/dfzwn.

References

Bangerth, W., et al. (2017), ASPECT v1.5.0, doi:10.5281/zenodo.344623. [Available at https://aspect.dealii.org/publications.html.]
Beucher, S., and C. Lantuéjoul (1979), Use of watersheds in contour detection, in *Proceedings International Workshop on Image Processing*, Real-Time Edge and Motion Detection/Estimation, pp. 17–21, Rennes, France, doi:citeulike-article-id:4083187.
Bird, P. (2003), An updated digital model of plate boundaries, *Geochem. Geophys. Geosyst.*, *4*(3), 1027, doi:10.1029/2001GC000252.
Coltice, N., M. Gérault, and M. Ulvrová (2017), A mantle convection perspective on global tectonics, *Earth Sci. Rev.*, *165*, 120–150, doi: 10.1016/j.earscirev.2016.11.006.
Canny, J. (1986), A computational approach to edge detection, *IEEE Trans. Pattern Anal. Mach. Intell.*, *6*, 679–698.
Crameri, F., and P. J. Tackley (2014), Spontaneous development of arcuate single-sided subduction in global 3-D mantle convection models with a free surface, *J. Geophys. Res. Solid Earth*, *119*, 5921–5942, doi:10.1002/2014JB010939.
Crameri, F., and P. J. Tackley (2015), Parameters controlling dynamically self-consistent plate tectonics and single-sided subduction in global models of mantle convection, *J. Geophys. Res. Solid Earth*, *120*, 3680–3706, doi:10.1002/2014JB011664.
Foley, B., and T. W. Becker (2009), Generation of plate-like behavior and mantle heterogeneity from a spherical, visco-plastic convection model, *Geochem. Geophys. Geosyst.*, *10*, Q08001, doi:10.1029/2009GC002378.
Gordon, R. G. (1998), The plate tectonic approximation: Plate nonrigidity, diffuse plate boundaries, and global plate reconstructions, *Annu. Rev. Earth Planet. Sci.*, *26*, 615–642, doi:10.1146/annurev.earth.26.1.615.
Mallard, C., N. Coltice, M. Seton, R. D. Muller, and P. J. Tackley (2016), Subduction controls the distribution and fragmentation of Earth's tectonic plates, *Nature*, *535*, 140–143, doi: 10.1038/nature17992.
Meyer, F. (1994), Topographic distance and watershed lines, *Signal Process.*, *38*, 113–125, doi:10.1016/0165-1684(94)90060-4.
Meyer, F. (2012), The watershed concept and its use in segmentation: A brief history February 2, arXiv:1202.0216v1
Meyer, F., and S. Beucher (1990), Morphological segmentation, *J. Vis. Commun. Image Represent.*, *1*(1), 21–46, doi:10.1016/1047-3203(90)90014-M.
Moresi, L., and V. Solomatov (1998), Mantle convection with a brittle lithosphere: Thoughts on the global tectonic styles of the Earth and Venus, *Geophys. J. Int.*, *133*, 669–682.
Morgan, W. J. (1968), Rises, trenches, great faults, and crustal blocks, *J. Geophys. Res.*, *73*, 1959–1982, doi:10.1016/0040-1951(91)90408-K.
Morra, G., M. Seton, L. Quevedo, and R. D. Müller (2013), Organization of the tectonic plates in the last 200 Myr, *Earth Planet. Sci. Lett.*, *373*, 93–101, doi:10.1016/j.epsl.2013. 04.020.
Najman, L., and M. Schmitt (1994), Watershed of a continuous function, *Signal Process.*, *38*(1), 99–112
Rolf, T., N. Coltice, and P. J. Tackley (2012), Linking continental drift, plate tectonics and the thermal state of the Earth's mantle, *Earth Planet Sci Lett.*, *351*, 134–146, doi:10.1016/j.epsl.2012.07.011.
Sethian, J. A. (1999), *Level Set Methods and Fast Marching Methods: Evolving Interfaces in Computational Geometry, Fluid Mechanics, Computer Vision, and Materials Science*, vol. 3, Cambridge University Press, Cambridge, U. K.
Stadler, G., M. Gurnis, C. Burstedde, L. C. Wilcox, L. Alistic, and O. Ghattas (2010), The dynamics of plate tectonics and mantle flow: From local to global scales, *Science*, *329*(5995), 1033–1038.
Stein, C., J. Schmalzl, and U. Hansen (2004), The effect of rheological parameters on plate behaviour in a self-consistent model of mantle convection, *Phys. Earth Planet. Inter.*, *142*, 225–255.
Tackley, P. J. (2000), Self-consistent generation of tectonic plates in time-dependent, three dimensional mantle convection simulations: 1. Pseudoplastic yielding, *Geochem. Geophys. Geosyst.*, *1*, 1026, doi:10.1016/S0012-821X(98)00029-6.
Tackley, P. J. (2008), Modelling compressible mantle convection with large viscosity contrasts in a three-dimensional spherical shell using the yin-yang grid, *Phys. Earth Planet. Inter.*, *171*(1):7–18, doi:10.1016/j.pepi.2008.08.005.
Trompert, R., and U. Hansen (1998), Mantle convection simulations with rheologies that generate plate-like behaviour, *Nature*, *395*, 686–689, doi:10.1038/27185.
Van Heck, H. J., and P. J. Tackley (2008), Planforms of self-consistently generated plates in 3D spherical geometry, *Geophys. Res. Lett.*, *35*, L19312, doi:10.1029/2008GL035190.
Dougherty, E. R. (1994), Morphological segmentation for textures and particles, *Digital image processing methods*, 43–102.
Wessel, P., W. H. F. Smith, R. Scharroo, J. F. Luis, and F. Wobbe (2013), Generic mapping tools: Improved version released, *EOS Trans. AGU*, *94*, 409–410, doi:10.1002/2013EO450001.
Williams, S. E., R. D. Müller, and T. C. W. Landgrebe (2012), An open-source software environment for visualizing and refining plate tectonic reconstructions using high-resolution geological and geophysical data sets, *GSA Today*, *22*, 4–9, doi:10.1130/GSATG139A.
Zhang, S., and C. O'Neill (2016) The early geodynamic evolution of Mars-type planets, *Icarus*, *265*, 187–208, doi:10.1016/j.icarus.2015.10.019.
Zhong S. J., M. Gurnis, and L. Moresi (1998), The role of faults, nonlinear rheology, and viscosity structure in generating plates from instantaneous mantle flow models, *J. Geophys. Res.*, *103*, 15255–15268, doi:10.1029/98JB00605.